TECTONIC RECONSTRUCTION OF THE ELLICE BASIN

A THESIS SUBMITTED TO THE GRADUATE DIVISION OF THE

UNIVERSITY OF HAWAIʻI AT MĀNOA IN PARTIAL FULFILLMENT OF

THE REQUIREMENTS FOR THE DEGREE OF

MASTER OF SCIENCE

IN

GEOLOGY AND GEOPHYSICS

OCTOBER 2018

By

Elizabeth Kathlene Benyshek

Thesis Committee:

Paul Wessel, Chairperson

Richard Hey

Fernando Martínez

ACKNOWLEDGEMENTS

A special thank you to Dean Brian Taylor for continuous guidance and collaboration during this project as well as the originator of the super-plateau hypothesis. Dean Taylor is not listed as a committee member but spent countless hours devoted to this project (with great enthusiasm I might add) for which I am incredibly grateful. I thank my advisor and committee chair Dr. Paul Wessel for valuable scientific mentorship and continuous encouragement, as well as the opportunity to be part of this work. I also thank my committee members Fernando Martínez and Richard Hey for assisting in the improvement of this work. Additional thanks are owed to the Captain, crew and science team of survey KM1609 including the OTG marine technicians. I am beyond appreciative of the support and encouragement from my peers at the University of Hawai'i at Mānoa. Funding for this project was provided by the National Science Foundation (grant number OCE-1458964).

ABSTRACT

The Ellice Basin is located in the south equatorial Pacific between the Ontong Java and Manihiki plateaus, two of the three major plateaus that were emplaced as part of the single largest oceanic plateau Ontong Java Nui (OJN). The emplacement of OJN was abruptly followed by the long normal magnetic period known as the Cretaceous Normal Superchron (CNS, 121-83 Ma). A large component of oceanic crust in the Pacific Basin was formed during the CNS and lacks magnetic reversal identifications that are usually used to constrain relative plate motion; therefore, it is necessary to adapt other reconstruction methods. Here, we describe the relict spreading system of the Ellice Basin utilizing new high-resolution bathymetric data acquired on survey KM1609 during December 2016-January 2017. Identifiable morphological spreading features are analyzed to qualitatively characterize the spreading system. Features such as multi-strand fracture zones and a dueling, overlapping spreading center support the inference that the Ellice Basin was a fast spreading (and fast slipping) spreading system, as well as the great extent and CNS age constraints of the basin. Directional analysis of the spreading fabric lineaments, specifically with respect to determining Euler poles of opening rotation, is also performed. Three main stages of spreading are identified in Ellice Basin. Spatially conjugate points symmetric about the spreading central zone are used to create pseudo-isochrons to aid in calculating rotation parameters for reconstructions. Stage 1 fracture zones trend generally E-W until a clockwise rotation of the spreading direction produced a transtensional system. Stage 2 fracture zones splayed 10-20° from Stage 1 fault strands while lengthening spreading ridges to produce zed pattern rhomboids. An offset of Stage 2 fracture zones evidences the presence of a Stage 3. Stage 3 appears to be the result of a counter-clockwise rotation of the

spreading direction shortly before spreading ceased. Basaltic rocks dredged from selected locations along the survey track are to be dated and will provide tighter temporal constraints on the evolution of Ellice Basin and therefore this interpretation. Our reconstructions suggest that there was an earlier opening event prior to our three identified stages that ultimately reconstructs the Ontong Java and Manihiki plateaus.

TABLE OF CONTENTS

LIST OF FIGURES

1. Introduction

1.1. Pacific Basin during the Cretaceous

The Pacific Basin holds the record of the fastest current spreading rates in the world as well as the highest total crustal production rates evident from magnetic anomaly lineations and the age distribution of large igneous provinces (LIPs; Larson, 1991; Nakanishi, 1992). The most concentrated time period of this increased hotspot activity and LIP emplacement was the Early Cretaceous (140-120 Ma; Müller et al., 2016). Immediately following this period was the beginning of the long normal magnetic polarity period known as the Cretaceous Normal Superchron (CNS; 121-83 Ma, Granot et al., 2012). Many tectonic processes aided the accommodation of this major mass and energy flux to the surface, including migrating triple junctions and fracturing that produced new plates and formed new ocean basins (Worthington et al., 2006). Understanding all the causes and consequences involved with this event is complicated by the lack of magnetic reversal identifications. The largest of the Pacific Cretaceous LIPs was the rapidly emplaced Ontong Java Nui (OJN; ~125 Ma), which included present day Ontong Java, Manihiki and Hikurangi plateaus (Taylor, 2006). Rift structures on the northeast and southeast of the Manihiki Plateau suggest that additional LIP fragments were originally part of the super-plateau. However, these were rafted onto the Farallon plate and the Phoenix plate, respectively, and have since been subducted beneath the South America and Antarctica (Viso et al., 2005). The great extent of this emplacement, with an area estimated to have exceeded 1% of the Earth's surface (Worthington et al., 2006), likely led to the reorganization of the Pacific–Phoenix–Farallon spreading system. The end of OJN formation accompanied the end of Phoenix magnetic lineations a little after M0 (120 Ma), at the beginning of the CNS. After

M0, the OJN is inferred to have split by dominantly E-W spreading between the Ontong Java and Manihiki plateaus in the Ellice Basin (Taylor, 2006; Chandler et al., 2012); whereas N-S spreading prevailed between the Manihiki and Hikurangi plateaus whose extinct spreading center is the Osbourn Trough (Billen & Stock, 2000; Seton el al., 2012). After the CNS, magnetic anomaly lineations to the east of Manihiki Plateau can be traced from C34n (83 Ma) to present (Figure 1; Nakanishi & Winterer, 1998).

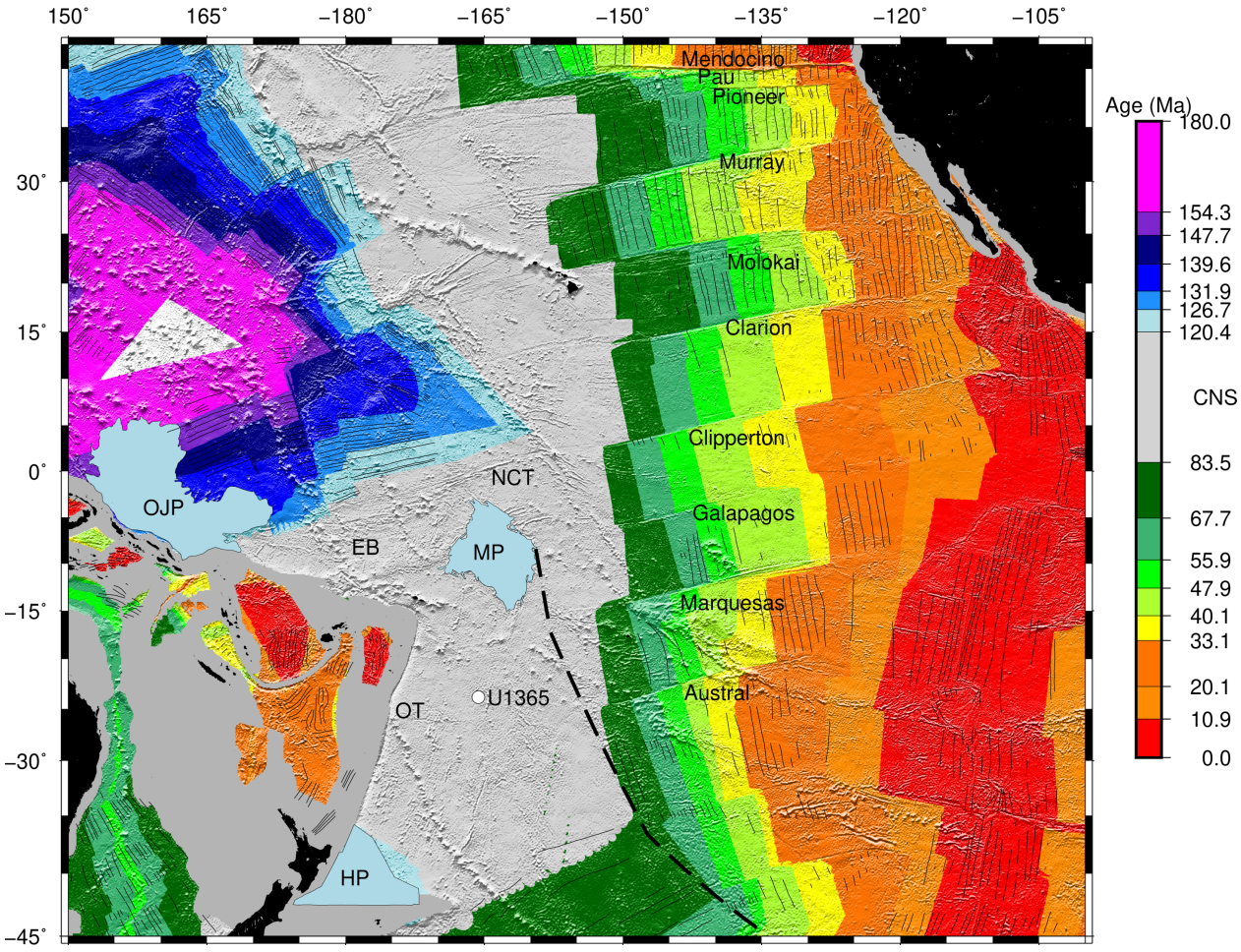

Figure 1: Age grid (Müller et al., 2016) shaded by predicted bathymetry (Sandwell et al., 2014), with M-series (Nakanishi et al., 1992) and Cretaceous (Cande et al., 1989) isochrons. Dashed black line represents Tongereva triple junction trace (Viso et al., 2005). White circle is IODP Expedition 329 Site U1365. OJP – Ontong Java Plateau, MP – Manihiki Plateau, HP – Hikurangi Plateau, EB – Ellice Basin, OT – Osbourn Trough, NCT – Nova Canton Trough.

1.2. Ontong Java Nui

Taylor (2006) used gravity-derived fracture zone identifications from satellite altimetry in conjunction with limited high-resolution multibeam bathymetry to identify seafloor spreading fabric in the CNS to propose the super-plateau hypothesis. Supporting evidence included similar geochemistry and seismic velocity structure across all three plateaus as well as shared formative volcanism at 125-119 Ma (Taylor, 2006). The breakup of OJN occurred via assumed contemporaneous spreading at the Osbourn Trough, between Manihiki and Hikurangi plateaus, and along ridges in the Ellice Basin, between Ontong Java and Manihiki plateaus. If rifting began immediately after formation, the earliest that spreading to create the Ellice Basin could have begun was ~119 Ma. Given the lack of magnetic anomaly reversal identifications in the Ellice Basin, the latest that spreading could have ceased was 83 Ma. The full separation between Ontong Java and Manihiki plateaus along fracture zones is ~3000 kilometers (Figure 1). This roughly calculates to a minimum average full spreading rate of ~85 mm/yr, but if spreading ceased earlier then average spreading rates would have been ~100 mm/yr.

A geophysical survey covering a wide swath across Osbourn Trough confirmed that it is an extinct spreading center (Billen & Stock, 2000) and not a recent crack in the Pacific plate (Small & Abbot, 1998). Billen & Stock (2000) estimated the cessation of spreading at the Osbourn Trough to be as recent as 71 Ma, which would indicate a relatively slow spreading rate for the system. However, Zhang and Li (2016) determined a very fast average full spreading rate of ~190 mm/yr between Manihiki and Hikurangi plateaus based on the dating of a recently recovered basement sample from Site U1365 of IODP Expedition 329 (103.7 Ma; Figure 1). Higher rates during the main phase of spreading are

also possible as the seafloor fabric near the extinct ridge has many hallmarks of slow-spreading systems, as deduced by Billen & Stock (2000) from their morphological analysis. Hence, these average spreading rates indicate that fast spreading ridge systems were producing seafloor between the major remnants of Ontong Java Nui. A recent survey and sampling of the Tuvalu seamount chain obtained anomalously high ages between 95-89 Ma near the central zone of the Ellice Basin (Finlayson et al., 2018). This suggests that spreading in Ellice Basin persisted later than spreading at the Osbourn Trough.

Chandler et al. (2012) developed a two-stage opening model utilizing high-resolution bathymetric data from a transit survey through central Ellice Basin (Figure 2) by the Korea Ocean Research and Development Institute (KORDI), in collaboration with the University of Hawai`i School of Ocean, Earth Science and Technology (SOEST). Chandler et al. (2012) solved for the best-fitting rotation utilizing the eastern margin of Ontong Java Plateau and the western margin of Manihiki Plateau. Fracture zones, which function as flowlines of past plate motion, were digitized from available bathymetric data in conjunction with 1 arc minute vertical gravity gradient (version 19.1, Sandwell & Smith (2009)) and 1 arc minute predicted bathymetry (Smith & Sandwell, 1997). The two-stage model allowed Chandler et al. (2012) to identify a central zone where extinct spreading centers not visible from satellite altimetry were assumed to be present.

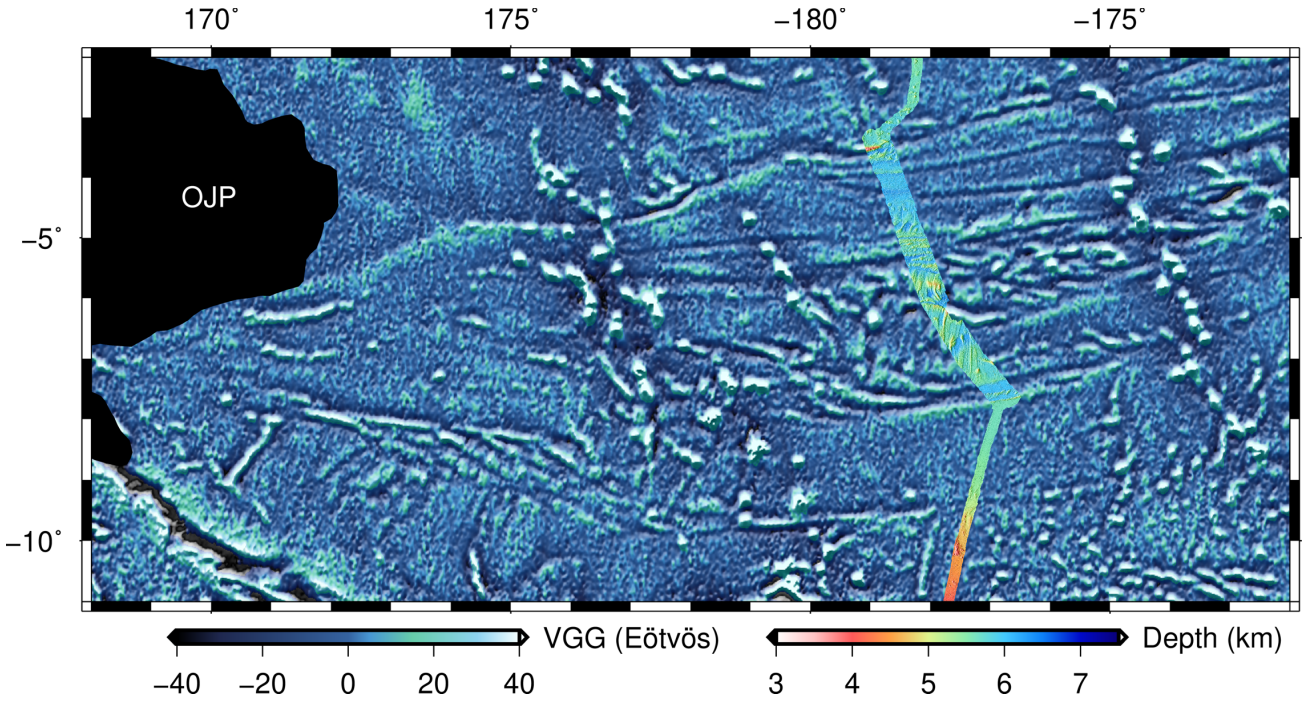

Figure 2: Vertical gravity gradient map (version 26, Sandwell et al., 2014) overlain with interpolated multibeam bathymetry obtained on KORDI NAP09-3 transit survey. OJP – Ontong Java Plateau.

1.3. Goal

This study relies on identifying characteristic spreading features from newly acquired high-resolution bathymetric data to understand the evolution of the Ellice Basin. Some of these features also provide noteworthy examples of processes that occur during changes of spreading direction that are applicable globally. Morphological and directional analyses of spreading fabric are utilized in lieu of magnetic anomaly identifications to distinguish stages and create pseudo-isochrons. Finite rotations are calculated based on pseudo-isochron selections and applied to bathymetric and satellite altimetry data to reconstruct the basin though time. Transitions between stages appear to have involved a complex interplay of rotating and propagating ridges and the rearrangement of closely spaced sets of right-stepping transform faults.

2. Survey KM1609

2.1. Objective

Survey KM1609 aboard the R/V *Kilo Moana* during December 4, 2016 – January 10, 2017 performed a reconnaissance survey of the central area of the Cretaceous Ellice Basin. The objective of the survey was to identify indicative spreading features to aid in the reconstruction of Pacific tectonics during the CNS, specifically the reconstruction of OJN, the world's single largest oceanic plateau. Survey areas were selected based on proximity to expected extinct spreading center locations inferred by Chandler et al. (2012). Over a period of 37 days, 7,500 nautical miles of multibeam bathymetry and sidescan sonar data were collected, concurrent with the collection of sub-bottom profiler records and underway gravity and magnetic data.

The newly acquired bathymetric data map ~59,000 square kilometers of the Ellice Basin and enable modifications to previously defined fracture zones that allow us to tighten the constraints on plate reorganization models. To understand the tectonic system, this study relies on identifying spreading fabric and characteristics at a scale below that identifiable from satellite altimetry (i.e., length scales of 10 km and smaller). Directional analysis of abyssal hill and fracture zone fabric is utilized to distinguish spreading stages. The formation of the Ellice Basin occurred within the time of the CNS, between 121-83 Ma. In order to provide additional age constraints on the Ellice Basin, we identified and dredged 16 targets during survey KM1609; suitable basalt samples will be $^{40}Ar/^{39}Ar$ age dated and reported in upcoming work by our colleagues at Oregon State University. Gabbro samples were also recovered from one dredge location that are to be zircon age dated.

2.2. Data Acquisition and Processing

The primary data utilized in this study are high-resolution multibeam bathymetry collected during survey KM1609. Data were collected using a Kongsberg Maritime EM122 12kHz multibeam echo sounder, which calculates a swath of seafloor depths from ping two-way travel times and estimates of sound velocity through the water column. Sound velocity profiles were updated at least twice a day during the survey using an expendable bathythermograph (XBT), which collects changes in water temperature verses depth to calculate sound velocity versus depth. Sidescan sonar data were produced based on the strength of ping returns to calculate reflectivity of the seafloor. Along track free air and magnetic data were collected using a Bell Aerospace BGM-3 gravity meter and a Geometrics G-882 cesium-vapor marine magnetometer. Seafloor sediment thickness records were collected using a 3.5 kHz sub-bottom profiler.

Bathymetric data were processed to reduce the influence of outliers using MB-System tools (Caress and Chayes, 1995) in conjunction with the Generic Mapping Tools (GMT; Wessel et al., 2013). Raw ".all" files were converted to usable MB-system format with ".mb59" file extension using the mbkongsbergpreprocess tool and reassembled into a manageable data list with the mbdatalist tool. Basic multibeam processing using the mbclean tool flagged beams that exceed a slope of 74 degrees or that are greater than ±20% of local median slope. Due to relatively high noise levels, additional pings were flagged using the interactive 3D visualization-based mbeditviz tool. Due to the angles of the transmitted ping fan, more noise appears on the outer edges of the swath (greater angle) than at the center beneath the ship (angle=0); these outer edges were also cleaned with the

mbeditviz tool. Flags were then applied using the mbprocess tool and new processed files with “p.mb59” extensions were created.

Processed data were gridded at 3 arc seconds based on the point spacing of raw data in the 4–6 km water depths encountered in the basin. Gridding was performed using the mbgrid tool with a weighted Gaussian average scheme. The grid spacing was chosen so that most bins would have at least three data points constraining the depth. From the resulting grids (Figure 3), it is readily observed that areas of raised topography and low sediment cover produced stronger returns and therefore yielded better coverage than areas of high sediment cover, which often are associated with voids in the grid. A thin plate spline interpolation scheme was used to fill data gaps up to 0.11 degrees wide to reduce this “Swiss cheese” effect and to allow for better visualization and more continuous interpolation and digitizing of lineaments. Sidescan sonar data were processed with the same parameters but using the mbmosaic tool for amplitudes.

Additional bathymetric data in the study region were obtained through the National Centers for Environmental Information (NCEI) Bathymetric Data Viewer and added to the total compilation grid. Data packages included a range of bathymetry file formats, but most files were provided in a usable MB-system format at the time of download. Older Seabeam files were converted to usable MB-system format with the mbcopy tool. All files that had not already been processed were run through the mbclean tool for basic processing; the resulting processing flags were applied with the mbprocess tool. For interactive viewing in GoogleEarth, a collection of PNG tiles were created with gradient shading (sunlight from 10° and 290°) and converted to KML format. This was especially helpful at sea for survey planning and adjustments (with pre-processed bathymetry data).

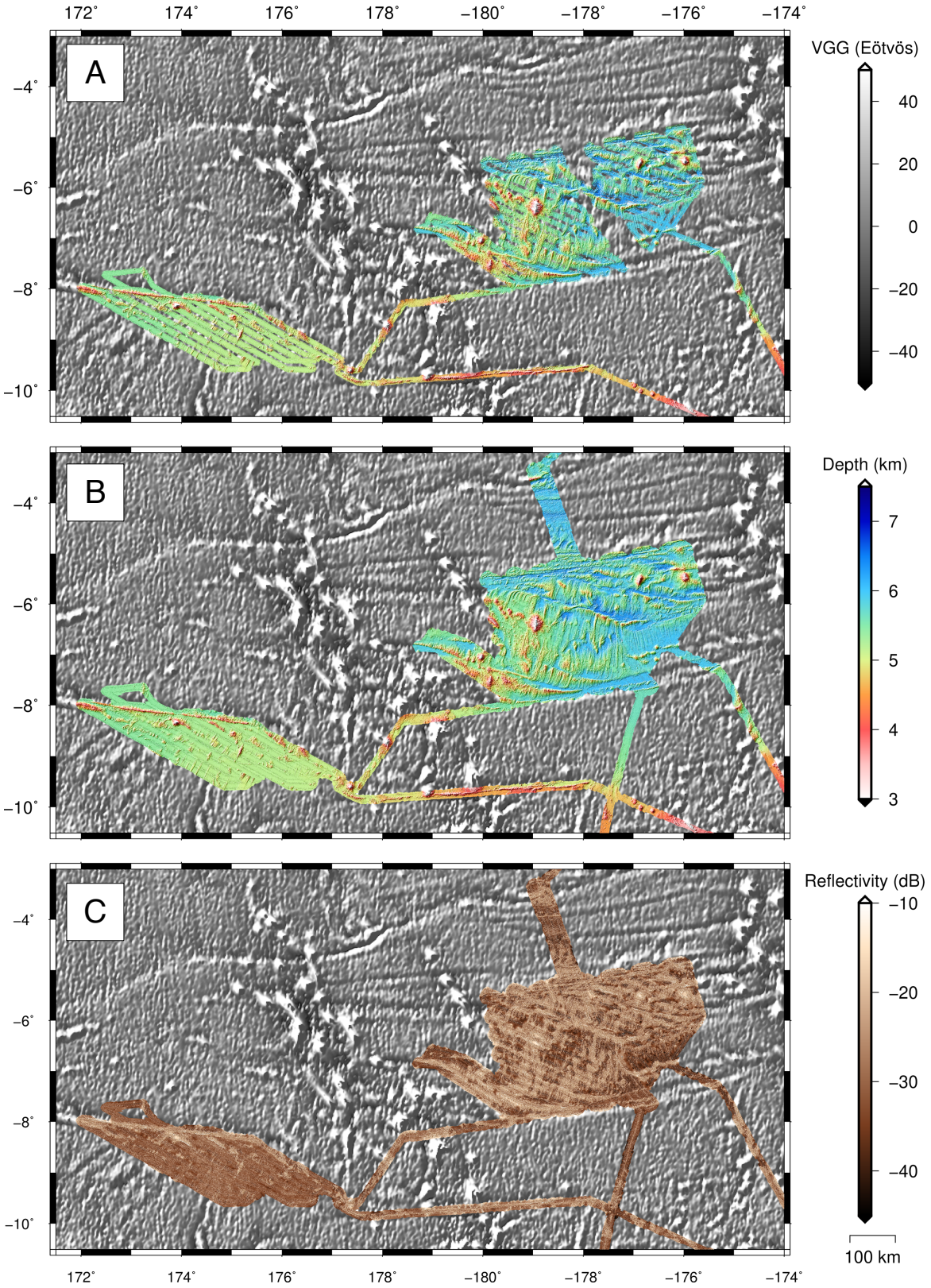

Figure 3: Vertical gravity gradient maps (version 26, Sandwell et al., 2014) overlain with high-resolution (3 arc sec) bathymetric data collected during survey KM1609. Map A displays raw gridded multibeam bathymetry, Map B displays thin-plate spline interpolation of gridded data with the KORDI survey added, and Map C displays interpolated sidescan sonar data.

3. First-order Discoveries

The new high-resolution bathymetric data collected during survey KM1609 mapped many features for the first time. Spreading fabric revealed by the previous KORDI transit survey was confirmed, but many of the deep fracture zone valleys that can be inferred from satellite altimetry are filled with sediments and were thus less prominent when mapped acoustically. In addition, many original seafloor features have been overprinted by tertiary volcanism that further complicates our study area (e.g. Finlayson et al., 2018).

3.1. Spreading Fabric

Survey KM1609 aimed to map extinct spreading centers in the Ellice Basin to aid in locating and characterizing the evolution of a past plate boundary. The survey revealed long fracture zones that can be traced point symmetrically about the central zone to the boundaries of the study area (Figure 3). These fracture zones bound abyssal hill fabric and confirm seafloor spreading in Ellice Basin as predicted by Taylor (2006). Other features associated with spreading systems that are observed in Ellice Basin include multi-strand fracture zones, a discontinuous overlapping and dueling spreading center, propagators and their conjugate pseudofaults, inside corner highs and corresponding outside corner low basins, and near-transform abyssal hill deflections (Fox & Gallo, 1983; Hey et al., 1980, Severinghaus & Macdonald, 1988; Croon et al., 2010).

3.2. Two Spreading Stages

Our mapping documented a rotation of the spreading direction from producing ~N- to producing ~NE-trending abyssal hills, supporting the two-stage Chandler et al. (2012) model. Stage 1 fracture zones trend generally E-W until a clockwise rotation of the spreading direction produced NW-SE trending fracture zones (Figure 3). This change in

spreading direction may have been associated with the collision of Hikurangi Plateau into the Gondwana subduction zone at Chatham Rise, which is considered to have led to the cessation of Osbourn spreading (Davy et al., 2008) and a major plate reorganization at ~105 – 100 Ma (Matthews et al., 2012). The survey also revealed an offset of the NW-SE trending fracture zones of Stage 2, indicating a late change in the direction of spreading almost back to Stage 1 trends. This change initiated a brief transpressional period just before spreading ultimately ceased.

3.3. Sediment Thickness

Due to the Cretaceous age of this basin, a thick layer of sediment has hidden structural details in deep, low-slope areas. New multibeam bathymetric data revealed a distinct difference in sediment thickness over the northeast region of the basin compared to the southwest region. The northeast region displayed relatively thin sediment cover and allowed for visibility of many complex morphological features, especially features of greater elevation. In contrast, sediment cover was revealed to be much thicker in the southwest region and features clearly visible from satellite altimetry are unseen in the bathymetry, such as a series of en-echelon gravity troughs (Figure 3, Map A). This contrast in sediment thickness is likely a regional effect of erosion of the island arc that was associated with the Vityaz trench to the south of the Ellice Basin.

4. Analysis

4.1. Seafloor Spreading

High-resolution multibeam bathymetric data allow for a detailed description of first-order morphological features of spreading in the Ellice Basin. The KM1609 survey may be

divided into two primary areas (Area A is located in the northeast region of Ellice Basin and Area B is in the southwest region) with the region between the two that has experienced considerable volcanic overprinting, such that its original seafloor fabric has largely been hidden by seamounts and volcanoclastic debris. Directional analysis of fracture zones and abyssal hill fabric aid in the selection of conjugate pseudo-isochrons and their connecting fracture zones, which are then used to calculate relative rotation poles for each stage of spreading mapped.

4.2. Morphological features

4.2.1. Rhomboids

The geometric structure of a spreading system provides direct evidence of changes in past plate motions (Searle et al., 1993). Changes in spreading direction are recorded by transform faults and preserved as fracture zones. When the spreading system experiences a change in spreading direction, the resulting geometry is usually a "Z" or "S" pattern rhomboid depending on the trend of the offset of the spreading ridges (left- or right-stepping) and the direction of rotation in relative plate motion (clockwise or counter-clockwise). When a primarily right-stepping spreading ridge system experiences a clockwise rotation of the spreading direction, as observed in Ellice Basin (Figure 3), the transforms open and create a transtensional system. If the rotation of the spreading direction is counterclockwise, the transforms close and a transpressional system is created and vice versa for left-stepping transform offsets (Atwater et al., 1993). Survey KM1609 mapped evidence of at least 11 "zed" pattern rhomboids (Figure 4), increasing numerically from northeast to southwest. Rhomboid limbs are point-symmetrically conjugate about the center of the spreading ridge.

Atwater et al. (1993) and Searle et al. (1993) both found that north Pacific fracture zones, such as the Molokai, Mendocino and Pau fracture zones, tended to consolidate transforms and lengthen spreading ridges when the system was transpressional and created new transforms and decreased the length of spreading ridges when the system was transtensional. Fracture zones in the Ellice Basin demonstrate an opposite transtensional situation than previously observed, but it is unclear why. Several transforms, at least three in our mapped area, were eliminated when the spreading direction changed, thereby increasing the length and decreasing the number of spreading centers. Propagation of the spreading ridges associated with termination of these transforms occurred late in the transition to Stage 2 and are associated with deformation and relocated crustal fragments between the extended and failed spreading ridges.

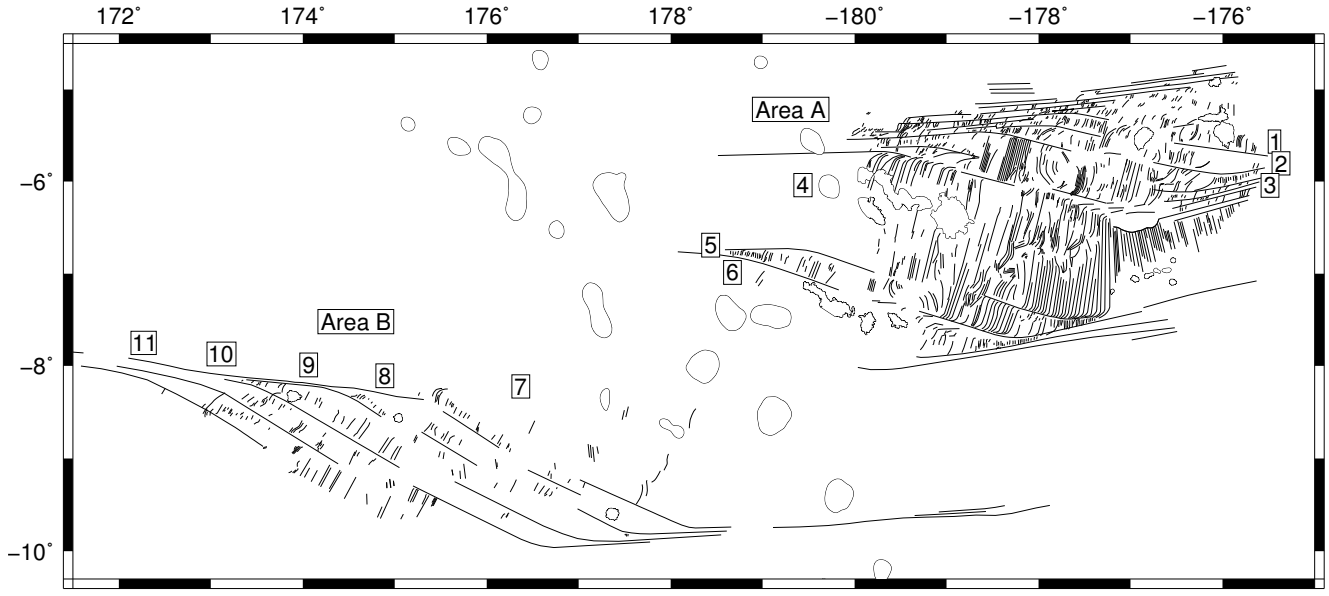

Figure 4: Line drawing interpretation of bathymetric data collected during survey KM1609. Rhomboids identified in Area A and Area B are labeled 1-11.

4.2.2. Multi-strand Fracture Zones

Survey KM1609 revealed Stage 1 fracture zones to consist of multiple closely spaced fault strands. The fault strands bound short, sigmoidal abyssal hills. Many Pacific fracture zones formed as multi-strand transform systems, so understanding how they evolve following changes in plate motion is vital to unraveling the history of the Pacific basin at large. Multi-strand fracture zones are common on fast spreading and fast slipping systems due to the easy migration of the spreading system on a thin, young plate (Fox & Gallo, 1983). Mapped multi-strand fracture zones in the Ellice Basin measure 40-50 kilometers in width and contain up to 9 fault strands spaced 3-20 kilometers apart. When the change in spreading direction occurred, spreading ridges extended in length and single fault transforms spaced 20-140 kilometers apart were created. From the vertical gravity gradient map (Figure 2), it appears that one large rhomboid separates Area A and Area B but it has been significantly overprinted by later volcanism. Stage 1 fault strands in Area B display greater relief and narrower spacing than those in Area A.

4.2.3. Dueling, Overlapping Spreading Center

In the case of Rhomboid 4, the conjugate limbs differ slightly due to a dueling, overlapping spreading center that propagated to the southwest and left a path of accreted transferred crust, which has a pseudofault conjugate of similar trend. While the eastern side of the propagator on the Manihiki plate was well mapped by survey KM1609, the conjugate western side on the Pacific plate was overprinted by volcanism and mapped in far less detail. This discontinuous propagation of the spreading center eventually took over spreading from the southerly adjacent Rhomboid 5. Prior to the initiation of the dueling, overlapping spreading center, the ridge reoriented and propagated north, taking out

multiple transforms in the process. This evolution was incredibly complex and resolving the accreted, transferred and rotated pieces of crust is difficult without magnetic reversal identifications. Though it is not entirely clear where the center of Rhomboid 4 is, it is clear that the dueling overlapping spreading center never creates new transforms but eliminates neighboring transforms instead.

Reorientation of the spreading ridges during a change in spreading direction can occur by rotation or propagation (Menard & Atwater, 1968; Hey et al., 1980), or synchronously as observed at Woodlark Basin spreading system (Goodliffe et al., 1997). Reorientation by rotation involves the gradual rotation of spreading centers as observed in the early transition from Stage 1 to Stage 2 in many of the rhomboids in Area A (Figure 4; Menard & Atwater, 1968). In the case of Rhomboid 4, the spreading center rotates on the southern end and propagates on the northern end. Reorientation by propagation involves the formation of a new spreading center with the new orientation propagating into older lithosphere with the old orientation and results in oblique pseudofaults that form a characteristic V-shape (Hey et al., 1980). Both modes of reorientation can be observed in the Ellice Basin usually involving inside corner highs and outside corner lows.

4.2.4. Inside Corner Highs

Inside corner highs form on the corner between a spreading ridge and an active transform as a result of decoupling in the transform that is associated with normal faulting and outside corner tilting that produces a topographic low (Severinghaus & Macdonald, 1988). Severinghaus and Macdonald (1988) concluded that inside corner highs only form on slow spreading ridges; however, we observe inside corner highs and their component outside corner lows in the Ellice Basin despite our inference of fast spreading. It is

important to note that the ridges adjacent to inside corner highs are relatively starved making the highs we observe distinctly different from intersection highs, which form on fast to intermediate spreading ridges (Gallo et al., 1986). Inside corner highs observed in the Ellice Basin occur during the rotation of the spreading direction from Stage 1 to Stage 2 and appear to have been a consequence of the transtensional environment that regimented the lengthening of the spreading ridges.

4.2.5. Abyssal Hill Deflections

Near-transform abyssal hill deflections are commonly found on both slow and fast spreading ridges as a result of a change in relative plate motion (Croon et al., 2010). Abyssal hill deflections, often referred to as J-shaped abyssal hills, are formed on the inside or outside corner of a ridge-transform intersection depending on whether the system is in transpression or transtension, respectively. Abyssal hills of Stage 2 exhibit J-shaped deflections opposite of inside corner highs. In two cases within Ellice Basin, J-shaped abyssal hill deflections appear to overshoot the fracture zone (Figure 4, Rhomboid 4). These features are consistent with the transtensional period of spreading during the transition from Stage 1 to Stage 2.

4.3. Directional Analysis

Bathymetric maps were generated using GMT and imported into Google Earth for digitizing and further analysis. Identifiable and representative abyssal hill and fracture zone lineaments from all stages were utilized. Lineations were selected based on continuity and extent of the lineaments and how well the fabric represents the spreading stage. Some abyssal hills were not digitized in entirety due to their near-transform deflections that do not directly exemplify the spreading direction (Fox & Gallo, 1984). Additionally, all

transitional fabric formed between two stages, and fabric deformed or relocated by the dueling propagator, were exempt from the directional analysis of the spreading stages. Due to the presence of Stage 3, Stage 1 and Stage 2 digitized spreading fabrics were further sub-divided into east and west limbs that are separated by the spreading central zone (Figure 5). For every stage of spreading, there is a corresponding Euler pole of rotation that describes the motion of that spreading, and it must lie somewhere on the great circle perpendicular to the small circles defined by transform faults or fracture zones (e.g., Wessel & Müller, 2017). Fracture zone and abyssal hill fabric lineaments from each stage were utilized with the GMT polespotter tool to find the poles that describe the trends of fabric on the present day seafloor.

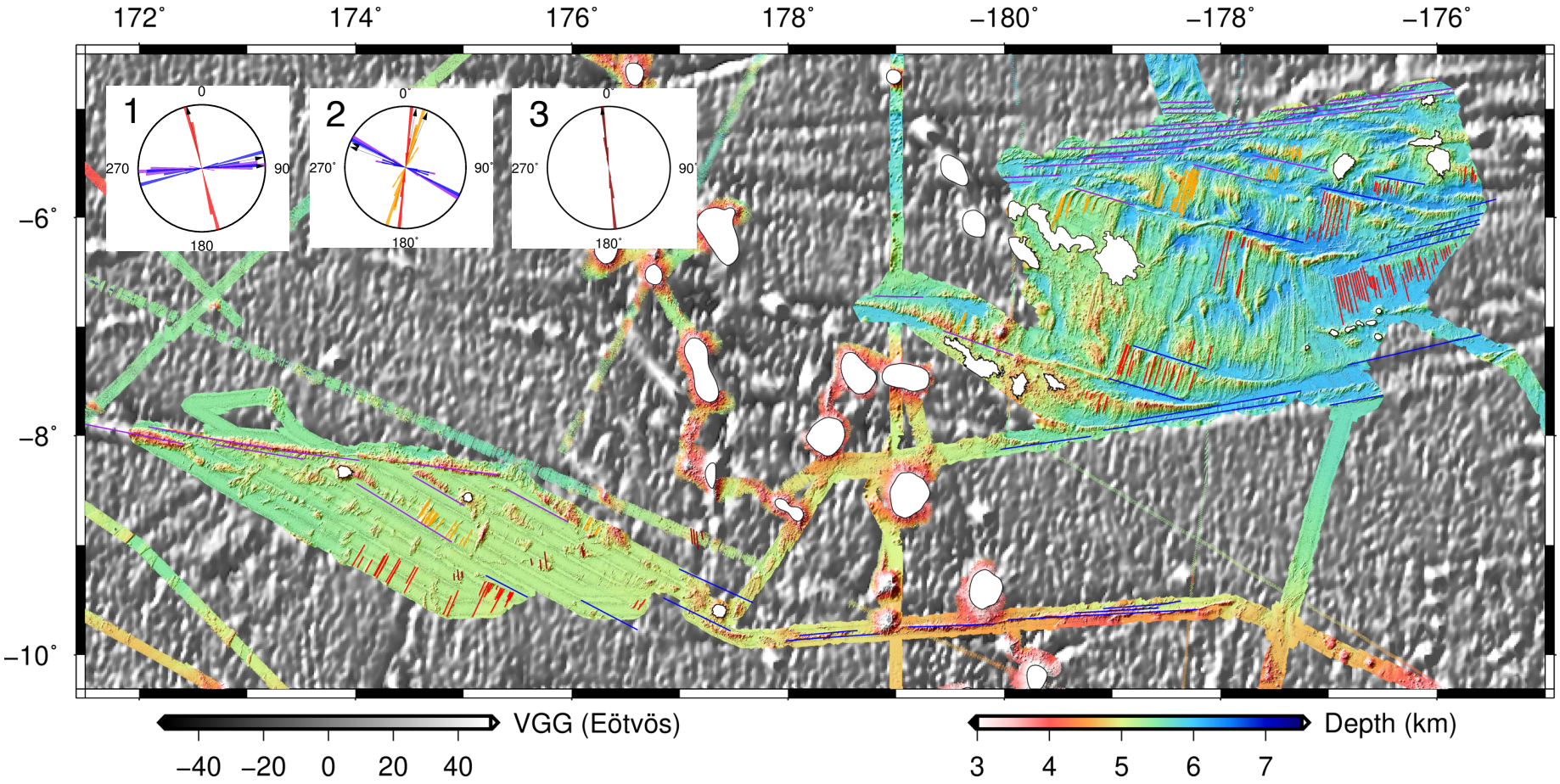

Figure 5: Vertical gravity gradient maps (version 26, Sandwell et al., 2014) overlain with interpolated multibeam bathymetry and digitized fracture zones (FZ) and abyssal hills (AH). Blue lines – east FZ, purple lines – west FZ, red lines – east AH, orange lines – west AH, dark red lines – Stage 3 AH, white polygons – seamounts. Line colors correspond to slice colors of inset rose diagrams. Average azimuths (black arrows) are as follows: Stage 1 – east FZ = 80°, east AH=346°, west FZ = 88°; Stage 2 – east FZ = 294°, east AH = 22°, west FZ = 290°, west AH = 11°; Stage 3 – AH = 353°.

4.3.1. Stage 1

The most distinguishable features of Stage 1 are the multi-strand fracture zones. Mapped multi-strand fracture zones are bundles of five or more fault strands and are connected by long spreading ridges 100 km and 176 km in length (Figure 5). Stage 1 fracture zones have an average azimuth of 80 and 88 degrees for east and west limbs, respectively. Spacing between fault strands within the bundles ranges from 3-10 km, but the abyssal hill fabric between them is sigmoidal and does not accurately represent the spreading direction. The only Stage 1 abyssal hill fabric that accurately represents the spreading direction is in the east limb of Rhomboid 4 before the overlapping spreading center initiates. The average azimuth of these east limb abyssal hills is 346 degrees. While the east and west limbs of Stage 1 are distinctly different in azimuth (Figure 5, Rose diagram 2), the azimuths of Area A and Area B also have distinct trends because of their proximity to the pole. The poles that represent the present data east and west Stage 1 spreading fabric are 176.4° W, 22.6° N and 178.8° W, 23.6° N, respectively.

4.3.2. Stage 2

The transition from Stage 1 to Stage 2 incorporated the transition from multi-strand to single strand fracture zones. Each multi-strand splays 10-20 degrees to a single strand, and in three cases transforms were eliminated as the new stage develops. It is important to note that this elimination occurs well into the transition at the beginning of steady Stage 2 fabric development. This transition lengthened and reoriented spreading ridges mostly by rotation of the spreading ridge until the onset of inside corner high and propagation development. Stage 2 spreading ridges range from 24-57 km in length, not including the discontinuous propagator that is composed of longer, dueling spreading centers. Stage 2

abyssal hills have an average azimuth of 22 degrees on the west and 11 degrees on the east. Stage 2 fracture zones have an average azimuth of 294 degrees on the west limbs and 290 degrees on the east limbs. The poles that represent the present data east and west Stage 2 spreading fabric are 174.1° E, 9.8° N and 175.3° E, 6.1° N, respectively.

4.3.3. Stage 3

The transition between Stage 2 and Stage 3 was the result of a counter-clockwise change of the spreading direction that put the system in a transpressional mode. Short ~N-trending abyssal hills can be identified in Area B but a thick layer of sediments covers most of the detail. Abyssal hill fabric of Stage 3 has an average azimuth of 353 degrees and are represented roughly by the pole 178.0° W, 17.7° N. This change in spreading direction returned the system to be dominated by short spreading ridges with long transform offsets. Spreading ridges in Area B are 10-20 km in length and are offset by up to 150 km. The continuity of Stage 3 features is more difficult to distinguish in Area A possibly due to closer vicinity to the pole of rotation. Their existence and net effect is marked by the left-lateral offset of the Stage 2 fracture zones. The Stage 3 period was brief and immediately followed by the extinction of the spreading system.

4.4. Poles of Rotation and Pseudo-isochrons

We seek to quantitatively reconstruct the Ellice Basin opening history as revealed by our seafloor survey. To that end, we will derive rotation parameters of relative opening for each of the seafloor spreading stages identified, noting that these may be extrapolated to areas of equivalent age that are not yet surveyed. Euler's theorem states that the motion of a rigid body on a sphere, such as a tectonic plate, can be described by an angular rotation about an axis through the center of that sphere (the pole of rotation). The relative motion

between two plates on either side of a spreading center is assumed to be parallel to the transform faults and, to first order, symmetric.

Pseudo-isochrons were selected based on conjugate features equidistant across the assumed spreading center. Poles representing present day spreading fabric for each stage were utilized for self-consistency in pseudo-isochron selection. For every stage of spreading, a total reconstruction pole is calculated to bring eastern pseudo-isochrons to their western conjugates. Pseudo-isochrons in conjunction with their offsetting fracture zones were utilized with the "hellinger1" program from the Ted Chang software suite (Kirkwood et al., 1999). In this method, the best-fit reconstruction is computed by minimizing the Hellinger (1981) criteria for the sum of the misfits of the conjugate sets with respect to individual great-circle segments. The main rules applied to the selection of pseudo-isochrons to be input into the hellinger1 program are as follows:

1.) Fractures and isochrons must be equivalent in length to their conjugate pair.
2.) Fractures and isochrons must be approximately orthogonal to their adjacent isochrons and fractures, respectively.
3.) Any change in opening must be monotonically decreasing toward the apparent pole of opening, proportional to sin(angle to pole).

The proper selection of conjugate sets is critical to the resulting rotation pole, so directional analysis of trends in spreading fabric were utilized to derive pseudo-isochron trends. Pseudo-isochrons and their rotation parameters are presented in a line model (Figure 6) where the youngest stage is consecutively removed from A – D. Unlike actual magnetic isochrons, the pseudo-isochrons are not guaranteed to represent the exact same age, though they do represent great circle segments about the stage pole that are

equidistant from the spreading axis, hence the uncertainty in the rotation poles are simply a relative measure of misfit.

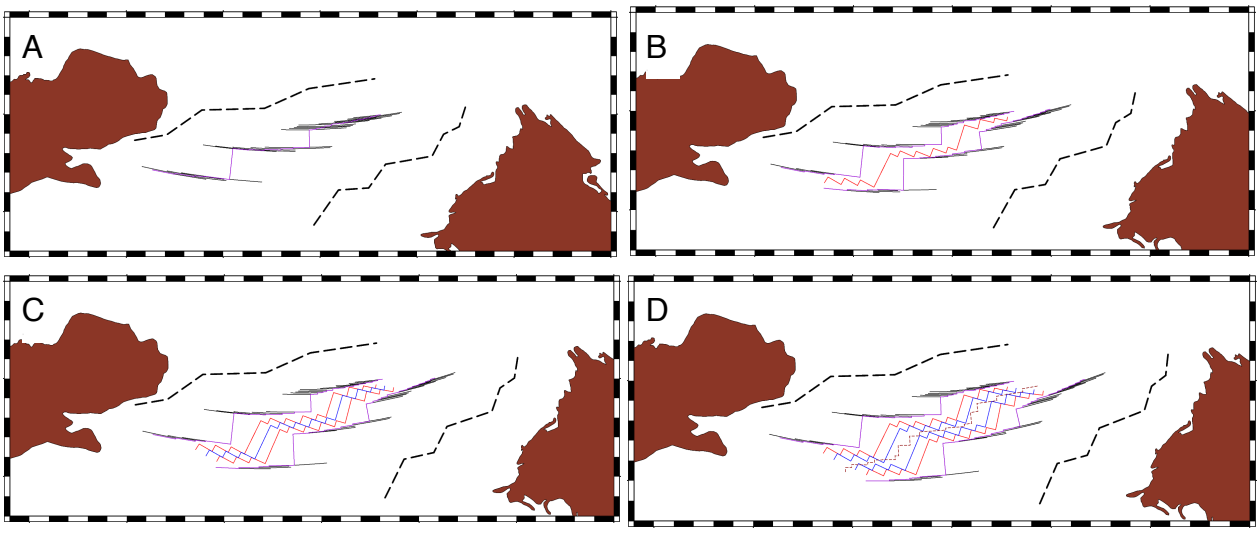

Figure 6: Line model of proposed spreading stages of Ellice Basin through time from Stage 1 (A) to current day (D). Purple lines – Stage 1 pseudo-isochrons, Red lines – Stage 2 beginning pseudo-isochrons, Blue lines – Stage 3 beginning/ Stage 2 ending pseudo-isochrons, dark red dashed line – late Stage 3 spreading center configuration.

5. Results

5.1. Ellice Basin Spreading System

Morphological analysis of the Ellice Basin provides evidence supporting fast spreading and fast slipping rates, such as a dueling, overlapping spreading center and multi-strand fracture zones. Based on our interpretation, this system experienced both a transtensional and a transpressional change in the opening kinematics. A key difference observed in the Ellice Basin compared to other Pacific fracture zones is the elimination of fault strands accompanying a transtensional change in spreading direction resulting in

longer and fewer spreading segments. The reason for this difference is not clear and perhaps is stochastic.

5.2. Multistage Formation

The two stages of spreading previously modeled by Chandler et al. (2012) are also evident in our analysis of gravity and multibeam bathymetry data. New bathymetric data collected during survey KM1609 revealed a third stage of spreading shown by short left-lateral offsets of Stage 2 fractures. The exact starting pseudo-isochrons for Stage 3 are difficult to characterize due to the proximity to the termination of spreading in Ellice Basin, though the total opening between them is constrained by the Stage 2 fracture zone offsets. Furthermore, observations of our Stage 1 reconstruction suggest that there exists a prior event that ultimately reconstructs Ontong Java and Manihiki plateaus together similar to but more complex than the Stage 1 modeled by Chandler et al. (2012) due to apparent crustal stretching (Hochmuth et al., 2016). Therefore, this interpretation can be further improved with additional high-resolution bathymetric data closer to the plateaus.

5.3. Reconstructions

Chandler et al. (2012) advanced the Taylor (2006) hypothesis by solving for spherical rotations based on inferred plateau boundaries of Ontong Java, Manihiki and Hikurangi plateaus. New high-resolution bathymetric data provide tighter constraints for the finite rotations that describe part of the opening of the Ellice Basin. Utilizing conjugate features, a series of finite rotations were calculated and applied to bathymetric and satellite altimetry data for Stage 1 – Stage 3 to reconstruct the central basin through time. These tectonic reconstructions allow for a better understanding of the evolution of the Ellice

Basin spreading system. In the following reconstructions, the Pacific plate with Ontong Java Plateau (the western plate) remains fixed.

Figure 7 presents all the pseudo-isochrons that were utilized in the following reconstructions. Spreading centers of the late Stage 3 are identified in Area B and the assumed ridge-transform configuration is presented (dark red dashed lines). The transpressional system created by a counter-clockwise rotation of the spreading direction forced transforms to cut across the existing configuration. The transition from Stage 2 to Stage 3 was rapid and poorly organized. Because of this, Stage 3 is removed (Figure 8) to the youngest distinguishable Stage 2 fabric (blue lines) and therefore likely includes a small component of the late Stage 2 opening as well. These pseudo-isochrons are roughly estimated to be 90-84 Ma based on available age constraints (Finlayson et al., 2018) and the constraints of CNS. Stage 2 spreading ridges are offset by transforms 44-87 km in length, which are generally shorter than their preceding Stage 1 transforms.

The next section removed contains all Stage 2 fabric that is formed after the transition from Stage 1 (Figure 9). These pseudo-isochrons (green lines) are estimated to correspond to a time around 100-95 Ma. This removal allowed for the analysis of the extended transitional period from Stage 1 to Stage 2. This stage represents a period of transtension for the spreading system when the number of transforms decreased as spreading ridges lengthened. As the spreading system adjusted to the new spreading direction, the outside corners of the ridge-transform intersection formed low basins as the spreading ridges attempted to reorient and lengthen while the inside corners formed highs possibly due to differences in local spreading rate along the reorienting ridge.

The reconstruction of Stage 1 removes all zed pattern rhomboids and three main multi-strand fracture zones remain (Figure 10). Assumed spreading ridges in these sections of closely spaced transforms range from 3-10 km in length and are offset by transforms 20-140 km in length. Stage 1 pseudo-isochrons (red lines) are estimated to be around 105-100 Ma. This reconstruction brings Ontong Java and Manihiki plateaus closer together but illustrates that the full opening history is more extended and complicated. Hochmuth et al. (2015) found the break-up of OJN to be complex including tectonic shearing and crustal stretching. The western margin of Manihiki Plateau specifically displays many features of crustal stretching based on the analysis of seismic data and this history can explain the asymmetry between suspected rift boundaries (black dashed lines).

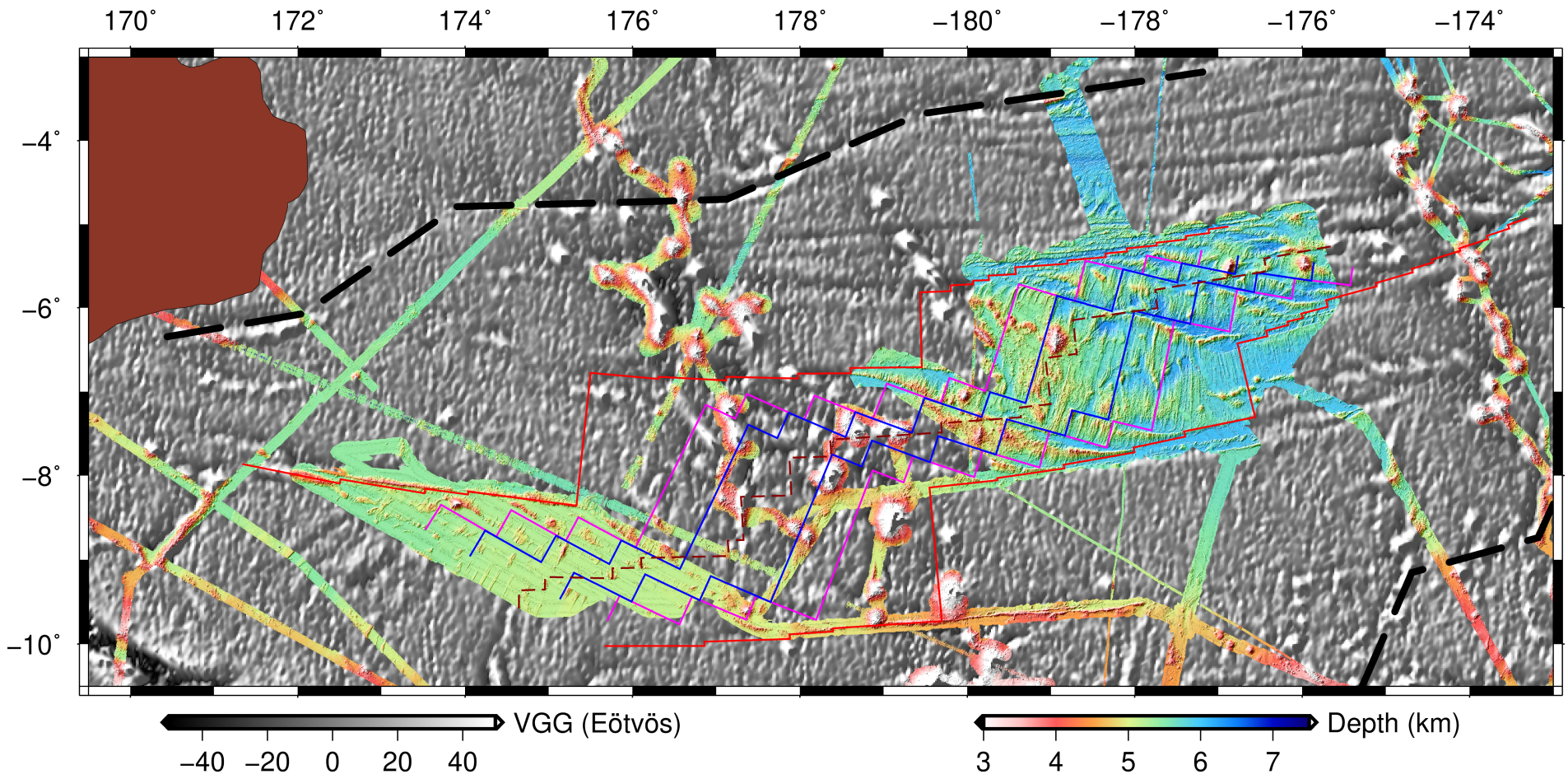

Figure 7: Vertical gravity gradient maps (version 26, Sandwell et al., 2014) overlain with interpolated multibeam bathymetry. Dark red polygons on the left and right borders represent Ontong Java and Manihiki plateaus, respectively. Black dashed lines – possible rift boundaries, red lines – Stage 1 pseudo-isochrons, Magenta lines – Stage 2 beginning pseudo-isochrons, Blue lines – Stage 3 beginning/ Stage 2 ending pseudo-isochrons, dark red dashed line – late Stage 3 spreading center configuration.

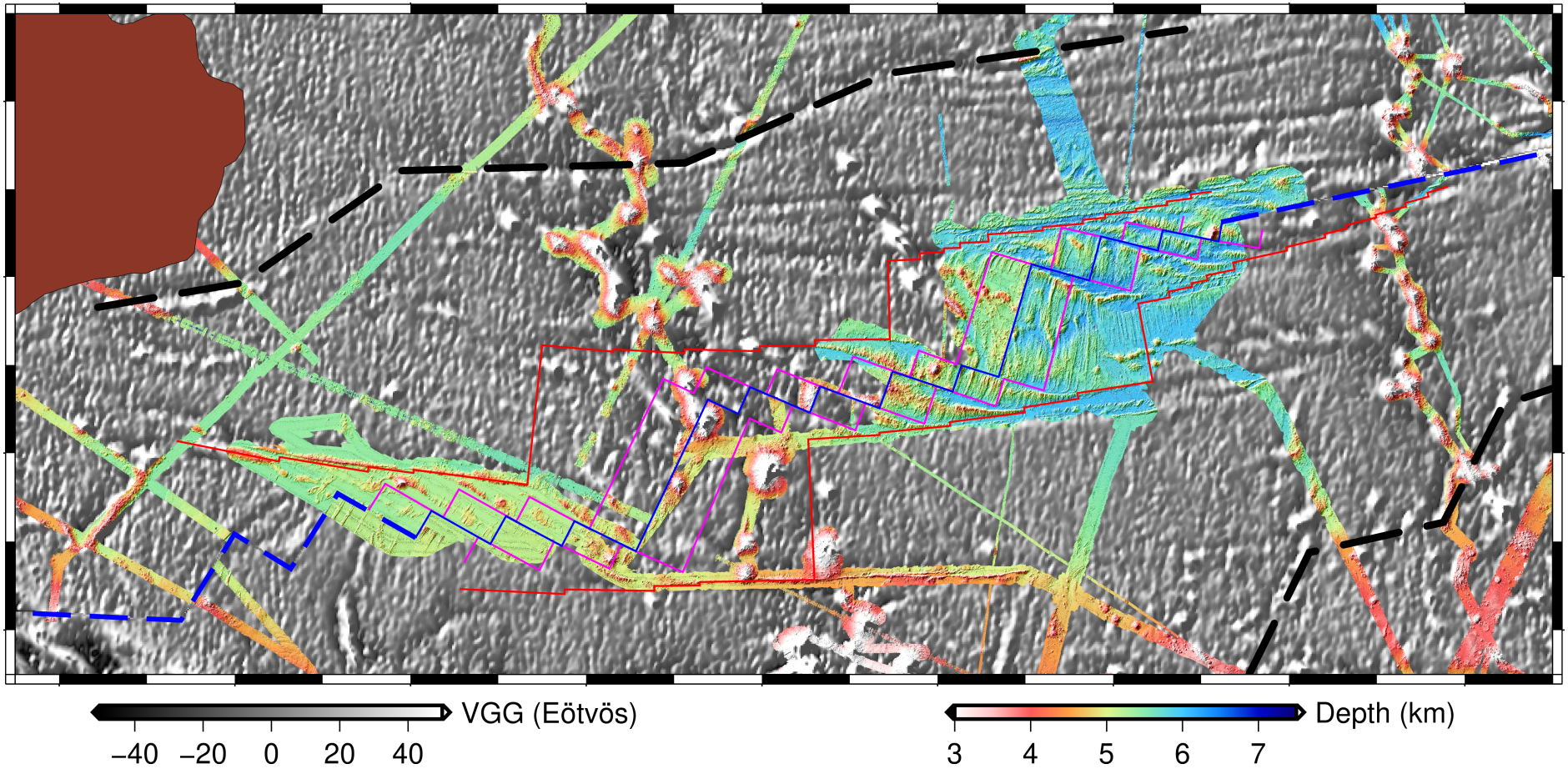

Figure 8: Vertical gravity gradient maps (version 26, Sandwell et al., 2014) overlain with interpolated multibeam bathymetry. Dark red polygons on the left and right borders represent Ontong Java and Manihiki plateaus, respectively. Black dashed lines – possible rift boundaries, red lines – Stage 1 pseudo-isochrons, Magenta lines – Stage 2 beginning pseudo-isochrons, Blue line – Stage 3 beginning/ Stage 2 ending pseudo-isochron, Blue dashed lines represent boundaries of the rotation that were not interpreted.

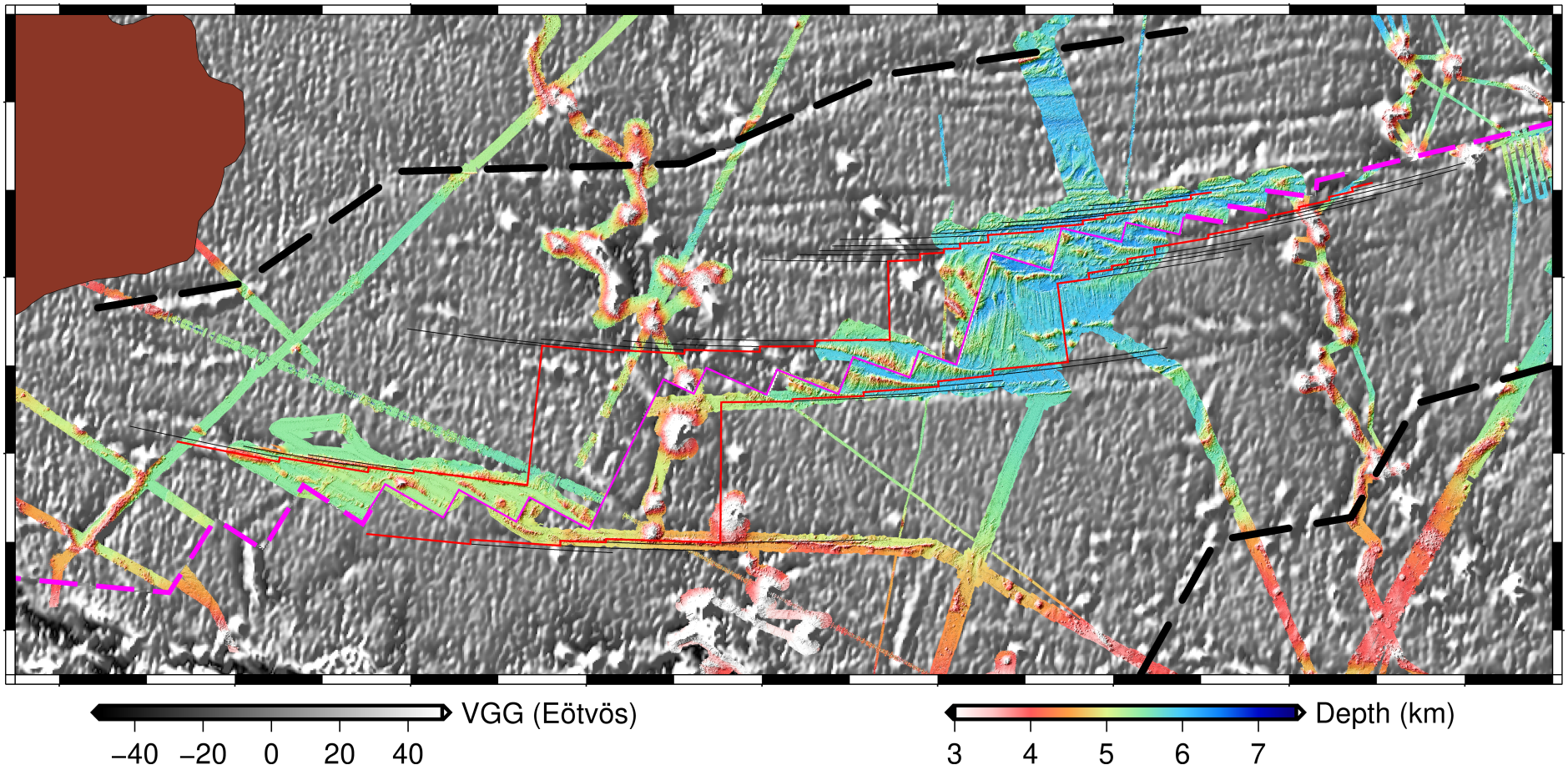

Figure 9: Vertical gravity gradient maps (version 26, Sandwell et al., 2014) overlain with interpolated multibeam bathymetry. Dark red polygons on the left and right borders represent Ontong Java and Manihiki plateaus, respectively. Black dashed lines – possible rift boundaries, red lines – Stage 1 pseudo-isochrons, thin black lines – flowlines of Stage 1, Magenta line – Stage 2 beginning pseudo-isochron, Magenta dashed lines represent boundaries of the rotation that were not interpreted.

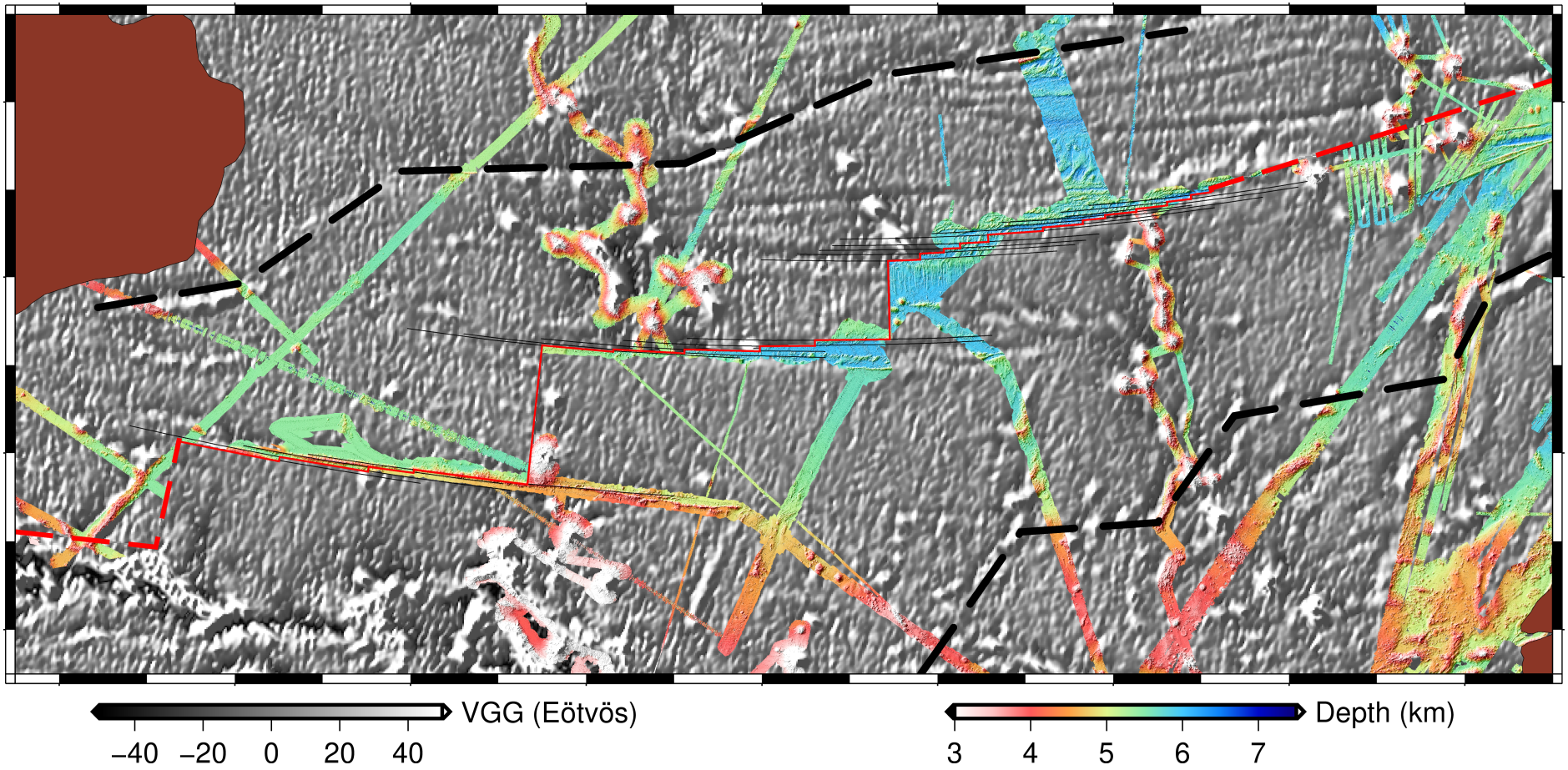

Figure 10: Vertical gravity gradient maps (version 26, Sandwell et al., 2014) overlain with interpolated multibeam bathymetry. Dark red polygons on the left and right borders represent Ontong Java and Manihiki plateaus, respectively. Black dashed lines – possible rift boundaries, thin black lines – flowlines of Stage 1, red line – Stage 1 pseudo-isochron, Red dashed lines represent boundaries of the rotation that were not interpreted.

6. Discussion

6.1. Variation from Chandler et al. 2012 Model

Newly acquired bathymetric data highlight a key difference between satellite altimetry and high-resolution bathymetric data sets. Seemingly single-strand fracture zones trending E-W in the satellite altimetry data were revealed to be multistrand with en echelon basins between strands creating a false trend when inferred from the lower resolution satellite altimetry data. As a result, there are slight variations from the previous Chandler et al. (2012) Stage 2 finite rotation and the finite rotations derived from this study. In addition, the Chandler et al. (2012) model fits Ontong Java and Manihiki plateau inferred boundaries back together, whereas this study only reconstructs to the end of Stage 1 (Figure 10), which compares well with the closing of Stage 2 in the Chandler et al. (2012, Figure 5) reconstruction. The three cyan stars identified in Figure 11 represent the total reconstruction poles obtained from this study. It is important to note that our Stage 1 reconstruction is the reconstruction back to the youngest Stage 1 spreading and our Stage 2 is reconstructed to observe the early transitional phase and oldest Stage 2 fabric. Our Stage 3 reconstruction is actually the reconstruction back to the youngest distinguishable Stage 2 fabric. This is why our results are similar only to the total Stage 2 reconstruction from the Chandler et al. (2012) model.

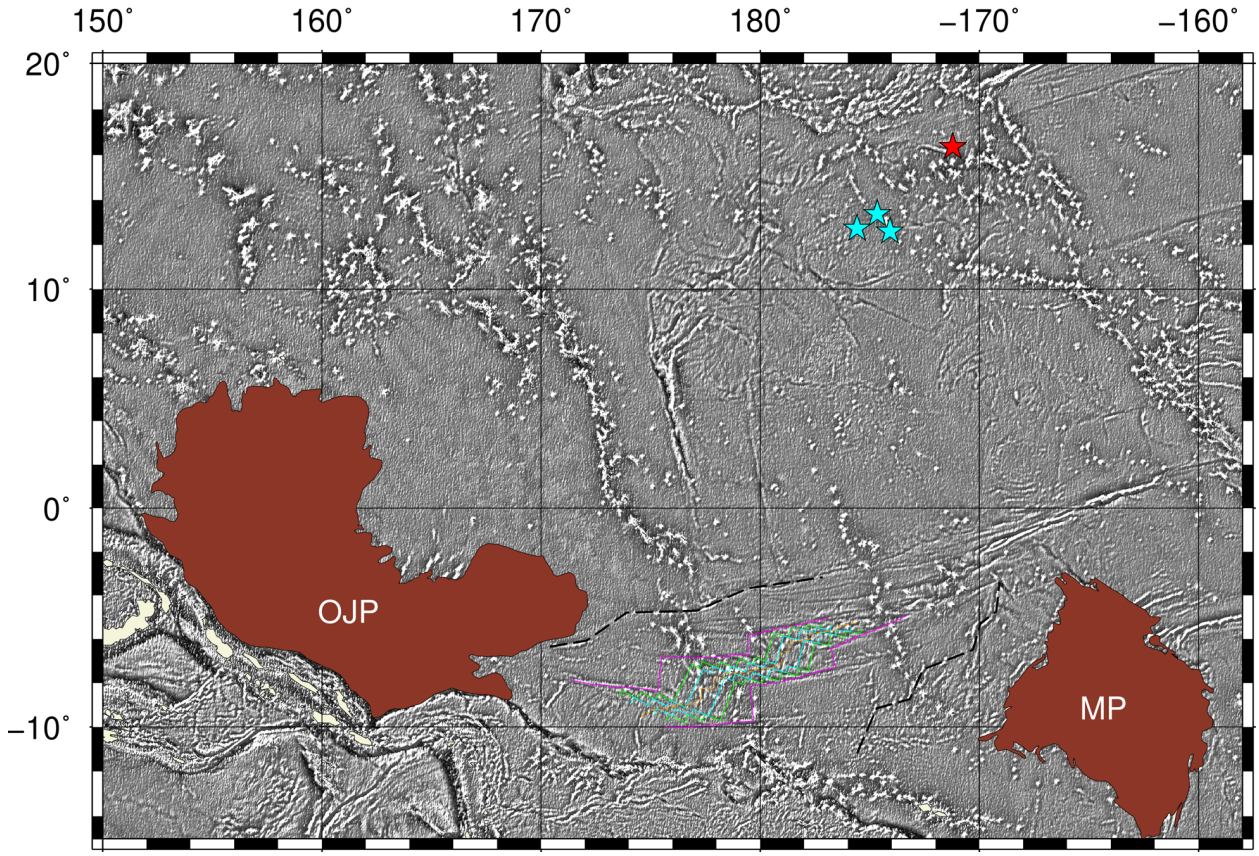

Figure 11: Vertical gravity gradient map (version 26, Sandwell et al., 2014) presenting Stage 2 pole location obtained from Chandler et al., 2012 (red star) and this study (cyan stars). OJP – Ontong Java Plateau, MP – Manihiki Plateau, Black dashed lines – Possible rift boundaries, Magenta lines – Stage 1 pseudo-isochrons, Green lines – Stage 2 beginning pseudo-isochrons, Cyan lines – Stage 3 beginning/ Stage 2 ending pseudo-isochrons, Orange dashed line – late Stage 3 spreading center configuration.

6.2. Other Conflicting Ideas

The confirmation of spreading in Ellice Basin conflicts with previous works that have recognized N-S fracture zones in the basin (Nakanishi et al., 1992; Hochmuth et al., 2015). In particular, Hochmuth et al. (2015) presents a magnetic anomaly map (Figure 5 in Hochmuth et al., 2015) that appears to have involved the insertion of assumed fracture zones from Nakanishi et al. (1992) to render an image that results in a false N-S trend

through the middle of Ellice Basin. Newly acquired data from survey KM1609 rules out such a trend.

6.3. Clipperton Ridge Jump

Judging from the seafloor fabric of Stage 3, spreading in the Ellice Basin does not appear to have slowed down significantly before extinction like at the Osbourn Trough. An explanation for this could be a ridge jump to the eastern side of the present Manihiki Plateau to the Clipperton fracture zone some time during the CNS. However, the presence of the Line Islands makes distinguishing a date for initial spreading parallel to the Clipperton fracture zone difficult. Additional data in this region, especially in the vicinity of the Nova Canton Trough (Figure 1), would aid in the determination of this event.

7. Conclusions

A.) Survey KM1609 revealed evidence for a past plate boundary between the Pacific Plate with Ontong Java Plateau and the Manihiki plate with the Manihiki Plateau. However, this boundary is in a complex arrangement due to a change in plate motion near (perhaps within <1My) the extinction of the spreading system. This stage was originally detected by a slight systematic offset between Stage 2 fractures that developed as a result of Stage 3 cross-cutting the system. Stage 3 appears to be the result of a counter-clockwise rotation of the spreading direction producing a short period of transpression before spreading ultimately ceased.

B.) Fast spreading rates are inferred for the Ellice Basin based on the great extent of the basin, plateau age constraints within the CNS and the near-central age dates

presented by Finlayson et al. (2018). Morphological features such as multi-transform fracture zones and a dueling, overlapping spreading center support this inference. Age dates presented by Finlayson et al. (2018) also suggest that spreading in the Ellice Basin persisted later than spreading at the Osbourn Trough.

C.) The Ellice Basin spreading system can be described by three main spreading stages as depicted from directional analysis of the fracture zones and abyssal hill fabric. Pseudo-isochrons were selected to obtain finite rotations for relative plate motion. Finite rotations were utilized to reconstruct Ellice Basin through time and revealed that the total tectonic history of the Ellice Basin cannot be described by three stages alone. Seismic data interpreted by Hochmuth et al. (2016) suggests significant crustal stretching on the western margin of Manihiki Plateau that could explain the asymmetry observed between the plateaus in our Stage 1 reconstruction. Therefore, this interpretation can be further improved with additional high-resolution bathymetric data closer to the plateaus.

D.) The spreading geometry of the Ellice Basin spreading systems demonstrates an opposite development than previously observed by Atwater et al. (1993) and Searle et al. (1993) on north Pacific fracture zones. The transtensional system of Ellice Basin, created by a clockwise rotation of the spreading direction on primarily right-stepping ridges, eliminated transforms as Stage 2 spreading developed. This lengthened and decreased the number of spreading ridges and increased the area formed within the rhomboids.

E.) Inside corner highs are primarily observed in the Ellice Basin during the transition from Stage 1 to Stage 2 and appear to be involved with the mode of reorientation. As the spreading ridge rotates to the new spreading direction, the outside corners of the ridge-transform intersection are relatively starved in their attempt to reorient and lengthen while the inside corners display a robust magma supply. This could be explained by conjugate asymmetric spreading about the ridge center during reorientation. Further examination of inside corner highs and their corresponding outside corner lows in other spreading systems is required to fully understand and corroborate this hypothesis.

REFERENCES

Atwater, T., Sclater, J., Sandwell, D., Severinghaus, J., Marlow, M.S. (1993). Fracture zone traces across the North Pacific Cretaceous Quiet Zone and their tectonic implications. The Mesozoic Pacific: Geology, tectonics, and volcanism. M. S. Pringle, W. W. Sager, W. V. Sliter and S. Stein. Washington, Am. Geophys. U.**:** 137–154.

Billen, M. I. and Stock, J. (2000). "Morphology and origin of the Osbourn Trough." J. Geophys. Res. **105**(B6): 13,481–413,489.

Cande, S. C., LaBrecque, J. L., Larson, R. L., Pitman, W. C., Golovchenko, X., and Haxby, W. F. (1989). Magnetic Lineations of the World's Ocean Basins. Tulsa, Okla., Am. Assoc. of Pet. Geol.

Caress, D.W., Chayes, D.N. (1995). "New software for processing sidescan data from sidescan-capable multibeam sonars." Proceedings of the IEEE Oceans 95 Conference: 997–1000.

Chandler, M.T., Wessel, P., Sager, W.W., (2013). "Analysis of Ontong Java Plateau palaeoloatitudes: evidence for large-scale rotation since 123 Ma?" Geophys. J. Int. **194**: 18–29.

Chandler, M.T., Wessel, P., Taylor, B., Seton, M., Kim, S.-S., and Hyeong, K. (2012). "Reconstructing Ontong Java Nui: Implications for Pacific absolute plate motion, hotspot drift and true polar wander." Earth and Planetary Science Letters **331-332**: 140–151. doi:10.1016/j.epsl.2012.03.017.

Croon, M. B., Cande, S. C., and Stock, J. M. (2010). "Abyssal hill deflections at Pacific-Antarctic ridge-transform intersections." Geochem. Geophys. Geosyst. **11**(11): Q11004.

Davy, B., Hoernle, K., Werner, R. (2008). "Hikurangi plateau: Crustal structure, rifted formation, and Gondwana subduction history." Geochem. Geophys. Geosyst. **9**(Q07004): doi:10.1029/2007GC001855.

Finlayson, V. A., Konter, J.G., Konrad, K., Koppers, A.A.P., Jackson, M.G., Rooney, T.O., (2018). "Sr–Pb–Nd–Hf isotopes and 40Ar/39Ar ages reveal a Hawaii–Emperor-style bend in the Rurutu hotspot." Earth and Planetary Science Letters **500**: 168–179.

Fox, P.J., Gallo, D.G. (1984). "A tectonic model for ridge-transform-ridge plate boundaries: Implications for the structure of the oceanic lithosphere." Tectonophysics **104**: 205–242.

Gallo, D.G., Fox, P.J., Macdonald, K.C. (1986). "A Sea Beam Investigation of the Clipperton Transform Fault: A Morphotectonic Expression of a Fast Slipping Transform Boundary." J. Geophys. Res. **91**(B3): 3455–3467.

Goodliffe, A.M., Taylor, B., Martínez, F., Hey, R., Maeda, K., Ohno, K. (1997). "Synchronous reorientation of the Woodlark Basin spreading center." Earth Planet Sci Lett **146**: 233–242.

Granot, R., Dyment, J., and Gallet, Y. (2012). "Geomagnetic field variability during the Cretaceous Normal Superchron." Nature Geoscience **5**: 220–223.

Hellinger, S.J. (1981). "The uncertainties of finite rotations in plate tectonics." J. Geophys. Res. **86**(B10): 9312–9318.

Hey, R.N., Duennebier, F.K., Morgan, W.J. (1980). "Propagating rifts on mid-ocean ridges." J. Geophys. Res. **85**: 3647–3658.

Hochmuth, K., Gohl, K., Uenzelmann-Neben, G. (2015). "Playing jigsaw with Large Igneous Provinces—A plate tectonic reconstruction of Ontong Java Nui, West Pacific." Geochem. Geophys. Geosyst. **16**(11): 3789–3807.

Kirkwood, B.H., Royer, J., Chang, T.C., Gordon, R.G. (1999). "Statistical tools for estimating and combining finite rotations and their uncertainties." Geophys. J. Int. **137**(2): 408-428.

Larson, R.L. (1991). "Latest pulse of Earth: Evidence for a mid-Cretaceous superplume." Geology **19**: 547–550.

Matthews, K.J., Seton, M., and Müller, R.D. (2012). "A global-scale plate reorganization event at 105–100 Ma." Earth and Planetary Science Letters **355–356**(0): 283-298.

Menard, H.W., Atwater, T. (1969). "Origin of fracture zone topography." Nature **222**: 1037–1040. doi:10.1038/ 2221037a0.

Müller, R.D., Seton, M., Zahirovic, S., Williams, S.E., Matthews, K.J., Wright, N.M., Shephard, G.E., Maloney, K.T., Barnett-Moore, N., Hosseinpour, M., Bower, D.J., Cannon, J. (2016). "Ocean basin evolution and global-scale plate reorganization events since Pangea breakup." Ann. Rev. Earth Planet. Sci. **44**(1): 107–138.

Nakanishi, M., Winterer, E.L. (1996). "Tectonic events of the Pacific plate related to formation of Ontong Java Plateau." Eos Trans. AGU **77**(46): F713.

Nakanishi, M., Tamaki, K., and Kobayashi, K. (1992). "Magnetic anomaly lineations from Late Jurassic to Early Cretaceous in the west-central Pacific Ocean." Geophys. J. Int. **109**: 701–719.

Sandwell, D. T., Müller, R. D., Smith, W. H. F., Garcia, E., Francis, R. (2014). "New global marine gravity model from CryoSat-2 and Jason-1 reveals buried tectonic structure." Science **346**(6205): 65-67. doi: 10.1126/science.1258213.

Searle, R.C., Holcomb, R.T., Wilson, J.B., Holmes, M.L., Whittington, R.J., Kappel, E.S., McGregor, B.A., Shor, A.N. (1993). The Molokai fracture zone near Hawaii, and the Late Cretaceous change in Pacific/Farallon spreading direction. The Mesozoic Pacific: Geology, tectonics, and volcanism. M. S. Pringle, W. W. Sager, W. V. Sliter and S. Stein. Washington, Am Geophys. U.**:** 155–169.

Seton, M., Müller, R.D., Zahirovic, S., Gaina, C., Torsvik, T., Shephard, G., Talsma, A., Gurnis, M., Turner, M., Chandler, M.T. (2012). "Global continental and ocean basin reconstructions since 200 Ma." Earth Science Reviews **113**: 212–270. doi:10.1016/j.earscirev.2012.03.002.

Severinghaus , F.P., Macdonald K.C. (1988). High inside corners at ridge-transform intersections. Mar. Geophys. Res.

Small, C. and D. Abbot (1998). "Subduction obstruction and the crack-up of the Pacific plate." Geology **26**(9): 795–798.

Smith, W. H. F., Sandwell, D.T. (1997). "Global sea floor topography from satellite altimetry and ship depth soundings." Science **277**(5334): 1956–1962.

Taylor, B. (2006). "The single largest oceanic plateau: Ontong Java-Manihiki-Hikurangi." Earth and Planetary Science Letters **241**(3-4): 372–380.

Viso, R.F., Larson, R.L., Pockalny, R.A. (2005). "Tectonic evolution of the Pacific-Phoenix-Farallon triple junction in the South Pacific Ocean." Earth and Planetary Science Letters **233**(1-2): 179.

Wessel, P., Müller, R.D. (2015). Plate Tectonics. Treatise on Geophysics, 2nd edition. G. Schubert. Amsterdam, Elsevier Ltd. **6:** 45–93.

Wessel, P., Smith, W.H.F., Scharroo, R., Luis, J.F., Wobbe, F. (2013). "Generic Mapping Tools: Improved version released." Eos Trans. AGU **94**(45): 409–410.

Worthington, T., Hekinian, R., Stoffers, P., Kuhn, T., Hauff, F. (2006). "Osbourn Trough: Structure, geochemistry and implications of a mid-Cretaceous paleospreading ridge in the South Pacific." Earth and Planetary Science Letters **245**: 685–701.

Zhang, G., Li, C. (2016). "Interactions of the Greater Ontong Java mantle plume component with the Osbourn Trough." Sci. Rep. **6**(37561).